Ceramics International 46 (2020) 15764–15771

Contents lists available at ScienceDirect

Ceramics International

journal homepage: www.elsevier.com/locate/ceramint

Highly sensitive C_2H_2 gas sensor based on Ag modified ZnO nanorods

Linsheng Zhou[a], Jihao Bai[a], Yueying Liu[a], Fengmin Liu[a,*], Hongtao Wang[a], Yiqun Zhang[a,b], Geyu Lu[a,**]

[a] State Key Laboratory on Integrated Optoelectronics, College of Electronic Science and Engineering, Jilin University, 2699 Qianjin Street, Changchun, Jilin Province, 130012, China

[b] College of Communication Engineering, Jilin University, Changchun, 130022, Jilin, China

ARTICLE INFO

Keywords:
Acetylene
Gas sensor
Ag modification
ZnO
Nanorods

ABSTRACT

The sliver (Ag) modified zinc oxide (ZnO) nanorods were successfully obtained with a simplified and environmentally friendly solvothermal method. Materials characterization indicated that the metallic Ag was located on the outside of ZnO nanorods after annealing. In comparison with ZnO nanorods, Ag modified ZnO (Ag–ZnO) nanorods exhibited a considerably enhanced response to C_2H_2. The response of the 3 at% Ag–ZnO based sensor operating at 175 °C is 539 (R_a/R_g), which is the highest value among all the sensors in detecting 100 ppm C_2H_2. The Ag–ZnO based sensors exhibited fast response speed, lower operation temperature and higher selectivity.

1. Introduction

C_2H_2 is a tintless, odorless, and extremely combustible gas, and plays a very important role in various industry applications [1–4] such as polyacetylene preparation, metal welding and conductive plastics preparation. Meanwhile, the fault of oil-immersed transformer can be evaluated by detecting C_2H_2 concentration [5–8]. Besides, C_2H_2 is also an extremely unstable gas and at risk of exploding in practical application. In order to sensitively and selectively detect C_2H_2, researchers have proposed many approaches such as infrared spectroscopy [9], gas chromatography [10], and solid electrochemical gas sensors [11]. Gas chromatography and infrared spectroscopy are generally limited to laboratory testing due to the large volume and high price, and ultra-high operation temperatures of all-solid mixed-potential-type gas sensor limit its application in many fields.

Semiconductor oxides based sensors have attracted wide attention and been developed rapidly due to high sensitivity, good repeatability, and easy fabrication. Especially, ZnO [12,13], SnO_2 [14–17], and TiO_2 [18,19] have been used in detecting various gases. Among these semiconductor oxides, ZnO is extensively studied in gas detecting due to easy fabrication, high mobility, and controllable morphology [20–22]. The performance of semiconductor oxides based sensors depends on the intrinsic, morphology, and modification of sensitive materials.

However, for pure semiconductor oxides materials, there are many shortcomings such as low sensitivity, high operation temperatures, high detection limit, and poor selectivity, which are difficult to meet the growing requirements in complex systems and harsh environments. Researchers have reported many ways to improve gas sensor performances. It has been proved that precious metal modification is an easy and efficacious solution.

In this paper, ZnO nanorods were synthesized and made into sensors. The properties of sensors were systematically investigated and optimized by a certain amounts of Ag modification. Among all the prepared samples, the 3 at% Ag–ZnO shows the highest sensitivity in detecting C_2H_2, meanwhile, it also has good selectivity and fast response speed. This work would play a significant role in monitoring C_2H_2 in many practical applications.

2. Experimental

2.1. Materials synthesis

The ZnO and Ag–ZnO nanorods were synthesized by using solvothermal method. A total of 2.98 mM of zinc nitrate hexahydrate > [$Zn(NO_3)_2 \cdot 6H_2O$] and various mole ratio (0%, 1%, 2%, and 3%) of sliver nitrate [$AgNO_3$] were added to 66 ml of absolute ethanol. Then, we added 3.576 g of NaOH and 10 ml of ethylenediamine and stirred the mixed solution. The mixed solution was then ultrasonicized and poured into a 100 ml solvothermal reactor and placed

* Corresponding author.
** Corresponding author.
E-mail address: liufm@jlu.edu.cn (F. Liu).

https://doi.org/10.1016/j.ceramint.2020.03.120
Received 16 January 2020; Received in revised form 6 March 2020; Accepted 11 March 2020
Available online 12 March 2020
0272-8842/

at 90 °C for 20 h to obtain the precursor. The precursor was then washed centrifugal for 4–6 times and dried at 60 °C and then annealed at 400 °C for 2 h. The final products were named as ZnO, 1 at% Ag–ZnO, 2 at% Ag–ZnO, and 3 at% Ag–ZnO, respectively.

2.2. Material characterization

X-ray diffraction (XRD, Rigaku D/max-2550, Cu Kα radiation, λ = 0.15418 nm) was used to examine the crystal structures of the samples. The morphology and nanostructure were analyzed by field-emission scanning electron microscopy (FESEM; JEOL JSM-7500F) and transmission electron microscopy (TEM; JEOL JSM-2100F). Energy dispersive X-ray spectrometry (EDS) patterns were observed through an attachment to TEM. The chemical state and composition of the elements was measured by X-ray photoemission spectroscopy (XPS) using an ESCALABMKII X-ray photoelectron spectrometer (Mg-Kα radiation, $h\nu$ = 1253.6 eV).

2.3. Fabrication and measurement of the sensors

The as-prepared materials were mixed with deionized water, brushed on the commercial substrate. The substrate coated with the sensing material was then dried for 30 min and annealed at 400 °C for 2 h. Finally, we inserted a resistance wire into substrate to provided operation temperatures of sensors. In the process of testing the sensors properties, the sensors were placed in tested gas or air, and compared the resistance changes that was exported and recorded though the apparatus. Define sensor sensitivity to gas as response with value of R_a/R_g, where R_a and R_g represented the resistance of sensors in air and test gas, respectively. The speed of gas detection by sensors was measured by response and recovery speed which referred to the time when the resistance of sensors reached 90% of the gross resistance variation in the process of absorbing and desorbing gas, respectively.

3. Results and discussions

3.1. Material characterization analysis

Fig. 1 gives the XRD patterns of synthesized materials. The results show the crystal structure of ZnO in pure materials and composite materials is hexagonal wurtzite (JCPDS File No.89–0511) [23–25]. For Ag–ZnO nanorods materials, there are three additional small peaks at

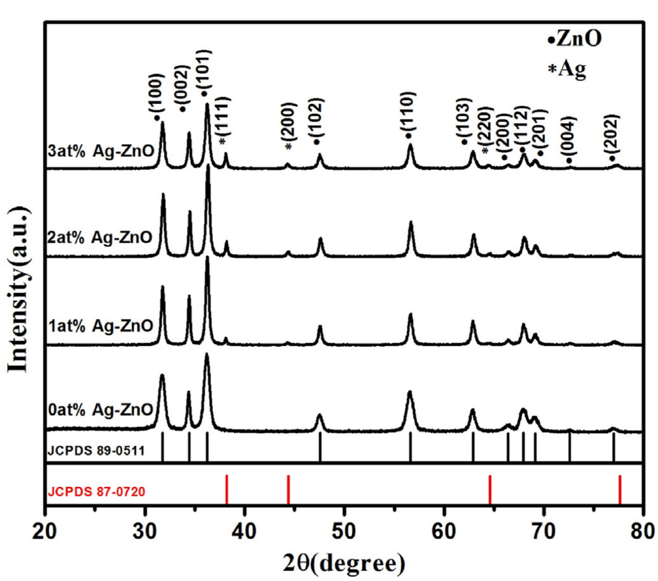

Fig. 1. XRD patterns of prepared samples.

38.2°, 44.2° and 64.6°, which were assigned to Ag (JCPDS File No.87–0720) [26–28]. The higher amount of $AgNO_3$ in the reactant is, the higher intensity of these three peaks is, which was in accordance with our experimental expectation. The eleven peaks belonging to ZnO in composite materials had no evident shift compared with pure ZnO, and thus metallic Ag was located on the outside of ZnO nanorods, unless the substitution of substituting Zn sites [29,30].

Fig. 2 shows the morphology features of prepared samples observed by SEM. Fig. 2a shows that some ZnO was composed of 20–50 nm diameter nanorods with lengths of several hundreds of nanometers, and other ZnO was rod-like particles. As shown in Fig. 2b-d, agglomerated nanoblocks were observed and suspected to be Ag particles. The FESEM images indicated that with the modification of Ag, the change in the ZnO microstructure was insignificant. More detailed information was further obtained by TEM shown in Fig. 3(a–d). Fig. 3b shows the (100) plane of ZnO with the interplanar spacing of 0.281 corresponding to the hexagonal wurtzite structure which was also observed in Fig. 3d corresponding to 3 at% Ag–ZnO samples, and another (111) plane of Ag with the interplanar spacing of 0.236 nm was observed in Fig. 3d. The distribution of O, Zn and Ag in 3 at% Ag–ZnO samples was analyzed by EDS. It could be found that O and Zn elements belonging to ZnO was well-distributed, and the nanoblocks mentioned above were the distribution of Ag.

Fig. 4 plots the Zn 2p, Ag 3d, and O 1s patterns from XPS measurement. In Fig. 4a, the binding energy of Zn $2p_{3/2}$ and Zn $2p_{1/2}$ was 1021.6 and 1044.6eV, respectively, which was identical to the value of ZnO and proved that Zn existed in the form of Zn^{2+} [31–33]. The modification of Ag had no effect on the XPS position of Zn 2p level. This result confirmed that metallic Ag was located on the outside of ZnO nanorods. Fig. 4b shows the Ag 3d patterns in 3 at% Ag–ZnO, the binding energy of 367.8 and 373.7eV related to Ag $3d_{5/2}$ and Ag $3d_{3/2}$, respectively, and the value was consistent with Ag^0 [34,35]. As shown in Fig. 4c and d, three peaks of O 1s located at 530, 531.2 and 532.1eV corresponding to crystal lattice oxygen (Zn–O), oxygen vacancy and chemisorbed oxygen species (H_2O, O_2), respectively [34,35]. Compared with ZnO, the content of oxygen vacancy and chemisorbed oxygen species increased from 25.7% to 28.8%–34.0% and 34.5% in 3 at% Ag–ZnO, respectively, this plays a great role in improving the sensing properties [36].

3.2. Gas sensing performance

Fig. 5a plots the response curve of as-prepared samples for detecting 100 ppm C_2H_2 in the temperature range from 125 to 300 °C. Fig. 5a shows that as the temperatures increases, the response of all sensors to C_2H_2 increases first and then decreases, so an optimum temperature was observed with a maximum response value. The highest response to 100 ppm C_2H_2 of the ZnO based sensor is 16, operating at 275 °C. With the modification of Ag, the response of the sensor was obviously improved. The greater the amount of silver, the more it increases. The champion device is the 3 at% Ag–ZnO based sensor in terms of response, which exhibits the highest response of 539 at 175 °C. Compared with ZnO based sensor, the operating temperature of champion device is reduced from 275 °C to 175 °C, and the response is increased by 33 times, which is an inspiring result.

Dynamic response curve of the ZnO based sensor to 100 ppm C_2H_2 operating at 275 °C is shown in Fig. 5b. The response and recovery speed were 15s and 87s, respectively, which is grudgingly acceptable. When measuring the dynamic response curve of 3 at% Ag–ZnO based sensor, which showed a very fast response speed of several seconds, but the recovery speed was closed to 1.5 h. Several seconds of response speed was ideal and lower than that of ZnO based sensor, but 1.5 h of recovery speed was too long and unacceptable for practical applications. Two solutions were proposed to shorten the long recovery speed: a. An appropriate high temperature was selected as the optimal operation temperature; b. The sensor worked at low temperature and

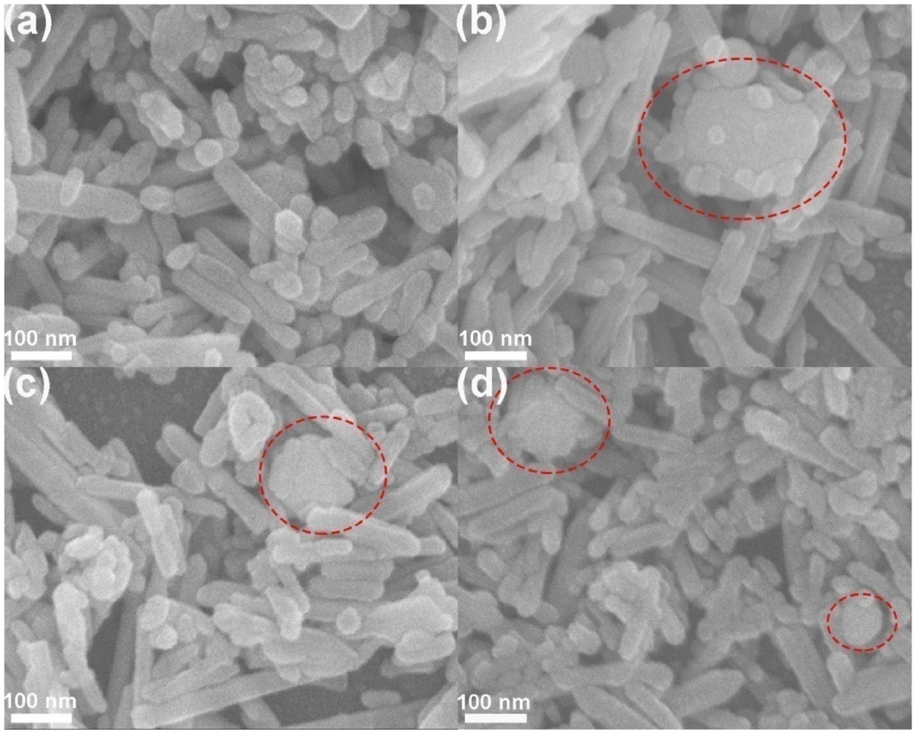

Fig. 2. SEM images of ZnO (a), 1 at% Ag-ZnO (b), 2 at% Ag -ZnO (c) and 3 at% Ag -ZnO (d).

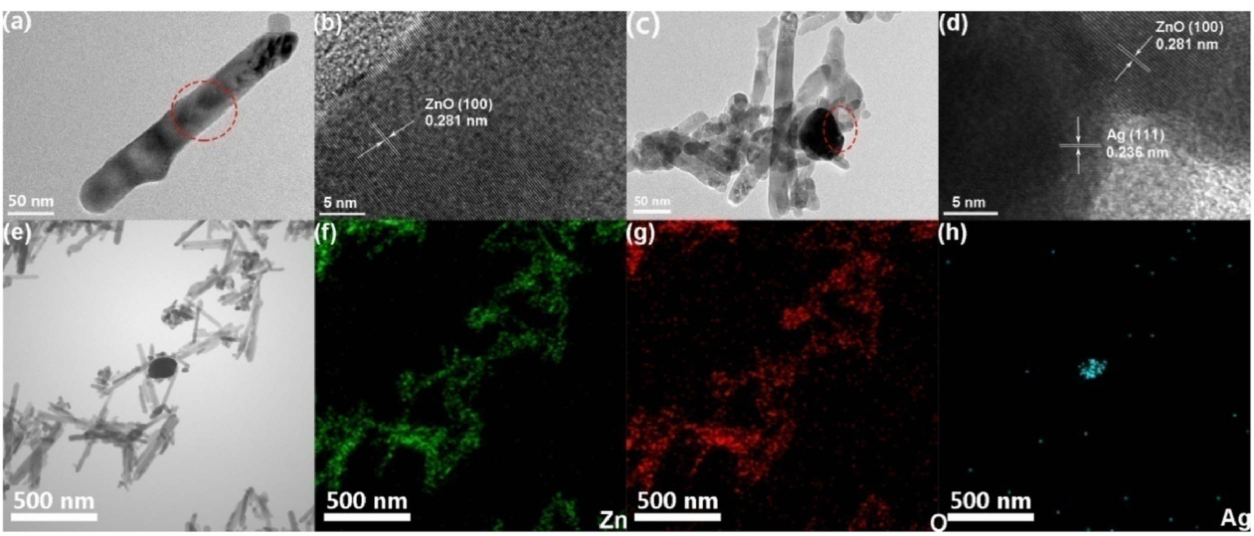

Fig. 3. TEM and HRTEM images of ZnO nanorods (a–b) and 3 at% Ag–ZnO nanorods (c–d); EDS results of 3 at% Ag–ZnO nanorods (e–h).

recovered at high temperature.

For the first solution, 250 °C was selected as operation temperature, and the corresponding response in detecting 100pmm C_2H_2 was 255 shown in Fig. 5a. The dynamic response curve was shown in Fig. 6a. The curve was smooth, and the result shows the response speed and recovery speed was approximately 6s and 200s, respectively. The response speed had no obvious change compared with that at 175 °C, but the recovery speed of the device decreased considerably. Fig. 6b shows the repeatability test of the sensor and the results shows that the device was basically stable and exhibited good repeatability. Fig. 6c shows the dynamic response curve for C_2H_2 with various concentrations from 1 to 1000 ppm, and the corresponding response ranged from 1.5 to 731.8. An overshoot effect was observed, that is, the sensor shows the supreme response when just placed in test gas, and then gradually reduced and stabilized at a value. The possible reason was that C_2H_2 reacted with oxygen in the air at a high temperature and C_2H_2 gas was partially burned.

In the second solution, the sensor operated at 175 °C and recovered at 300 °C. Fig. 7a shows the testing process. The sensor's resistance was stable in air at 175 °C. When C_2H_2 was introduced, the resistance gradually decreased and then stabilized, and the response speed was 6 s. After a period of time, the sensor was placed in the air again and the temperature was raised to 300 °C to accelerate the desorption of C_2H_2. When the resistance was stabilized again, the temperature was decreased to 175 °C. It could be found that the resistance increased firstly, then decreased, and finally stabilized. For semiconductor, the electron concentration reduced with the decrease of temperature, which was a very rapid process, so the resistance rose sharply first. Meanwhile, this process was the process of O_2 re-adsorption in the air. When the temperature decreased, the amount of oxygen adsorbed also decreased, and

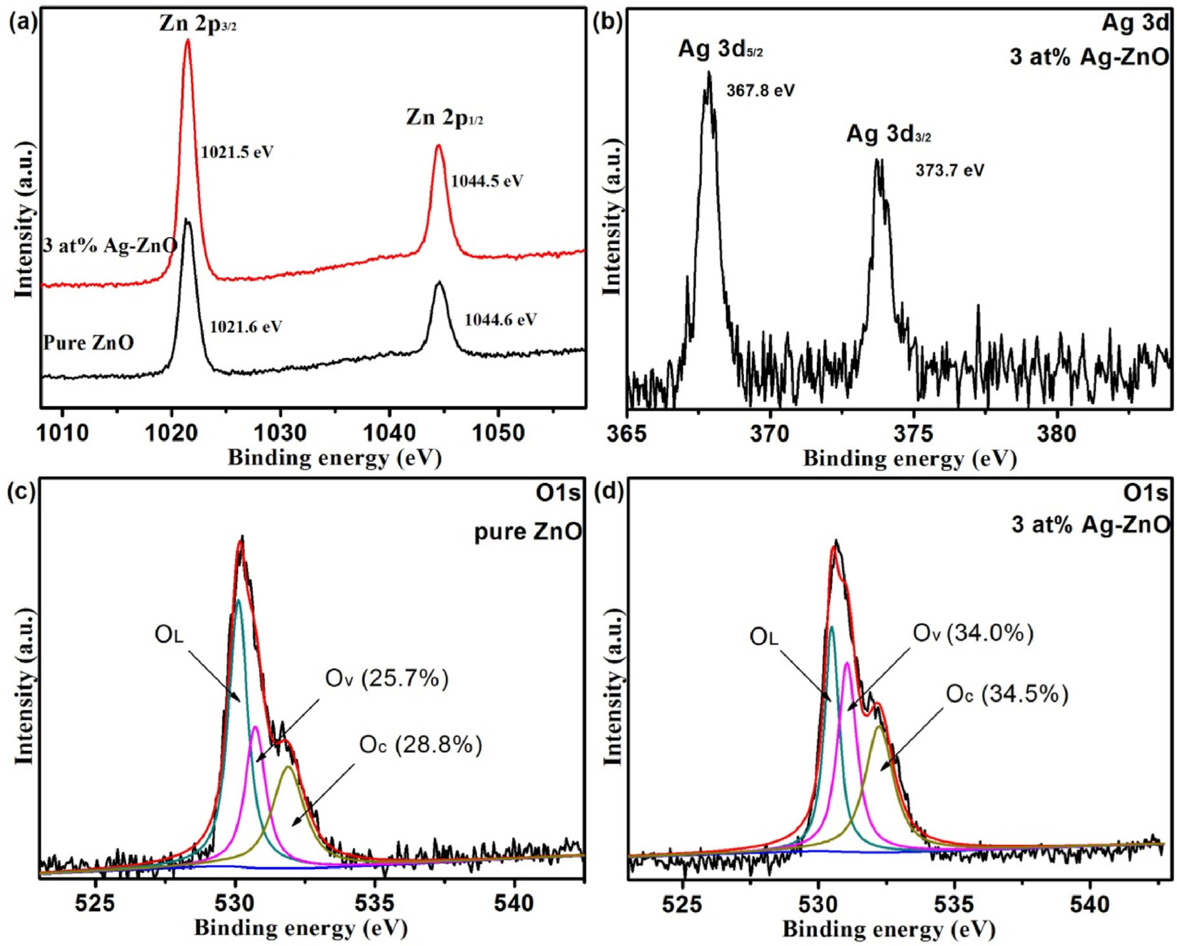

Fig. 4. XPS spectra of as-prepared samples: Zn 2p (a), Ag 3d (b), and O 1s (c–d).

the bound electrons were retransmitted to the semiconductor, so the resistance reduced and finally stabilized. Using this solution, the recovery speed of the sensor could be reduced to approximately 0.5 h. Fig. 7b shows the repeatability test, and the results shows that the device was basically stable and exhibited good repeatability.

Fig. 8a shows a broken-line diagram of the 3 at% Ag–ZnO based sensor's response to various concentrations of C_2H_2 at different temperature corresponding to the two solutions mentioned above. For the same C_2H_2 concentration, the response of 3 at% Ag–ZnO based sensor at 250 °C was significantly lower than that at175 °C and tended to be saturated earlier, and the response curve slope at 250 °C was much lower than that at 175 °C.

Fig. 8b shows the response to ten kinds of testing gases with concentration of 100 ppm. The test gases included C_2H_2, C_2H_4, H_2, CO, C_2H_5OH, CH_3COCH_3, CH_3OH, HCHO, C_6H_6, and C_7H_8. The results show that the response of the 3 at% Ag–ZnO based sensor to C_2H_2 is much higher than that of other nine kinds of gases. The selectively of the 3 at % Ag–ZnO based sensor at operation temperature of 175 °C is the

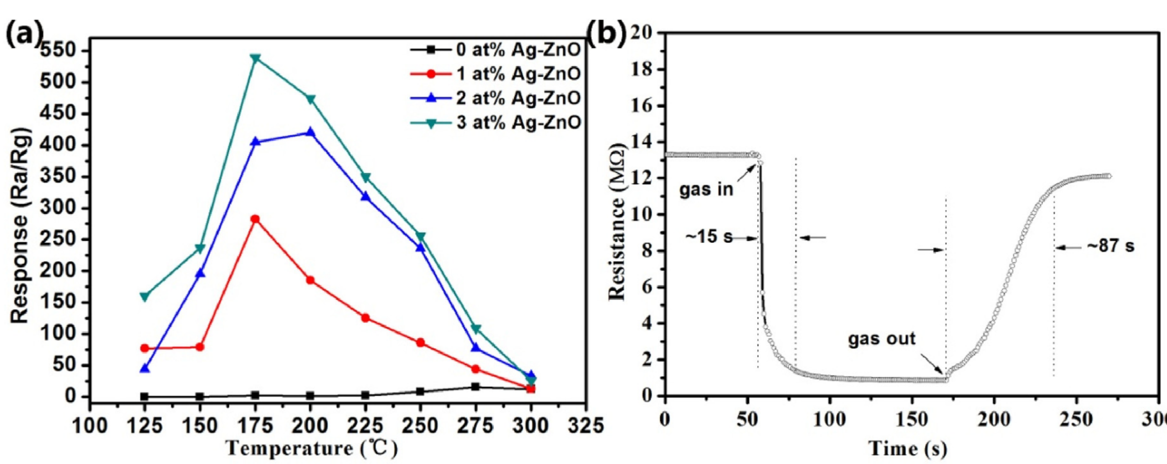

Fig. 5. Response to 100 ppm C_2H_2 at different operation temperatures of prepared materials (a); dynamic response curve for 100 ppm C_2H_2 of ZnO based sensor at 275 °C (b).

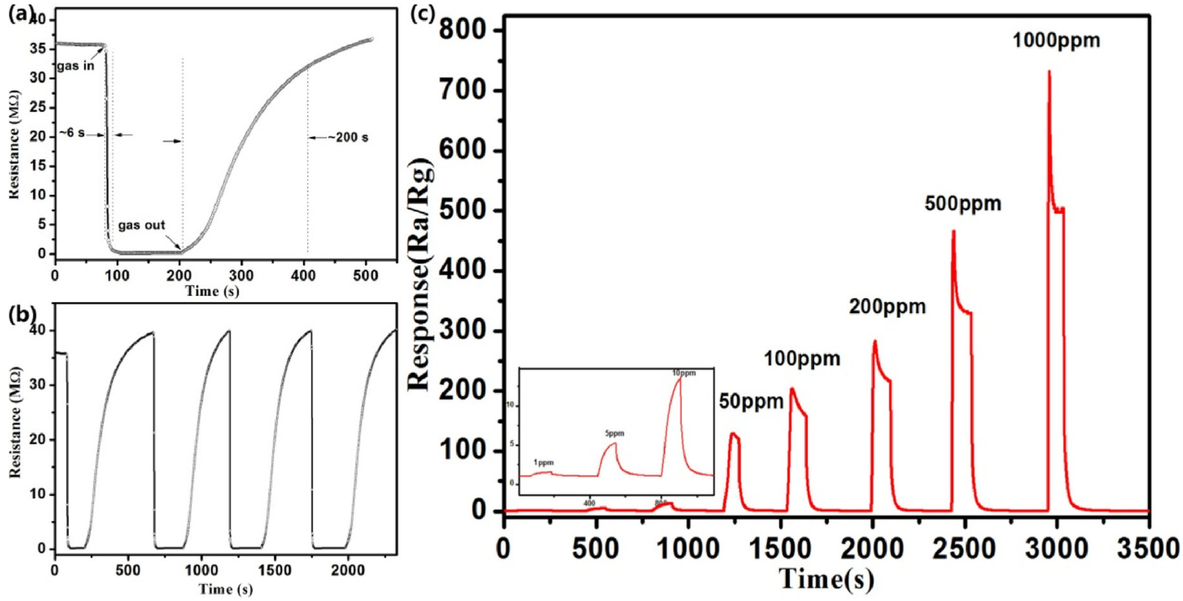

Fig. 6. Dynamic response curve for 100 ppm C_2H_2 (a); continuous response curves to 100 ppm C_2H_2 (b); dynamic response curve for different C_2H_2 concentrations (c) of 3 at% Ag -ZnO based sensor at 250 °C.

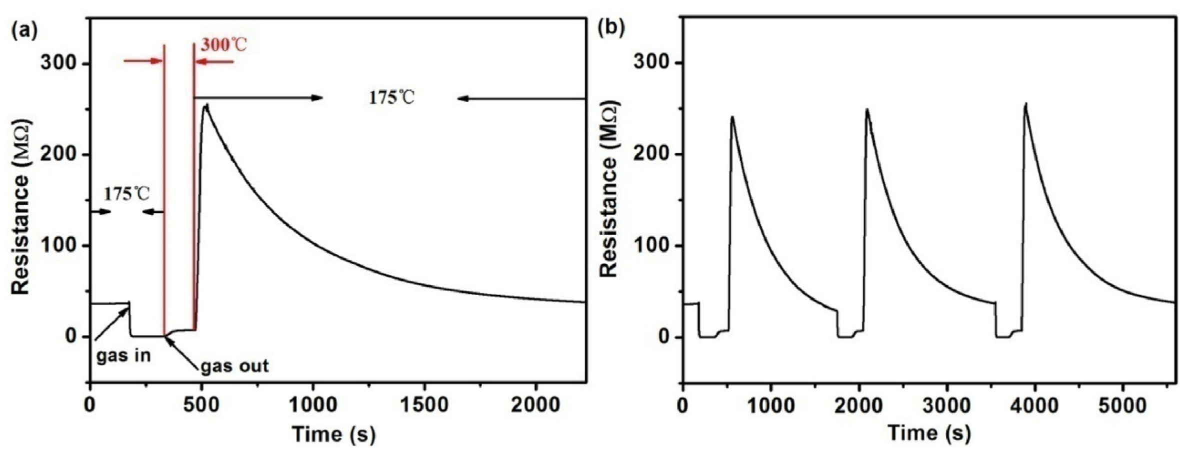

Fig. 7. Dynamic response (175 °C) - recovery (250 °C) curves (a); continuous response curves (b) to 100 ppm C_2H_2 of 3 at% Ag–ZnO based sensor.

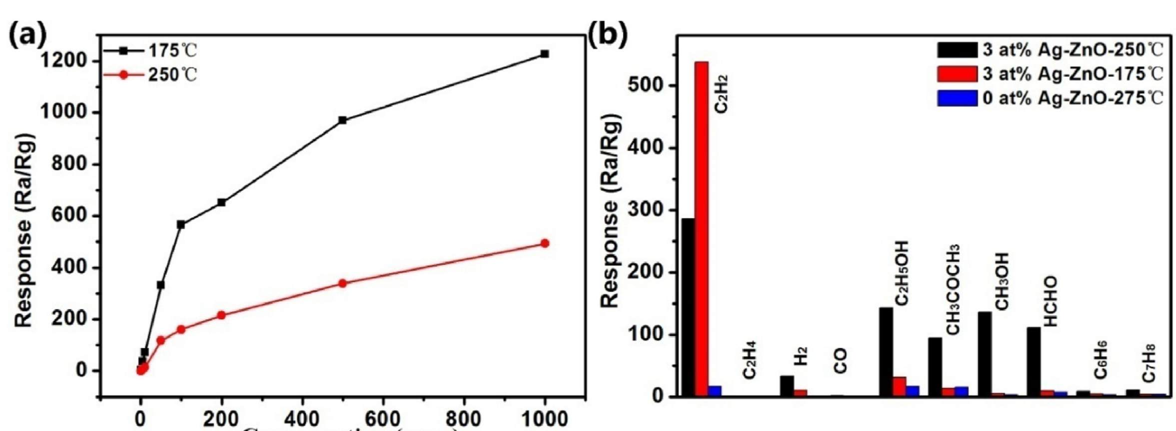

Fig. 8. Response of 3 at% Ag–ZnO based sensor to various concentrations of C_2H_2 (a); response to various gases of ZnO (at 275 °C) and 3 at% Ag–ZnO based sensors (at 175 °C and 250 °C) (b).

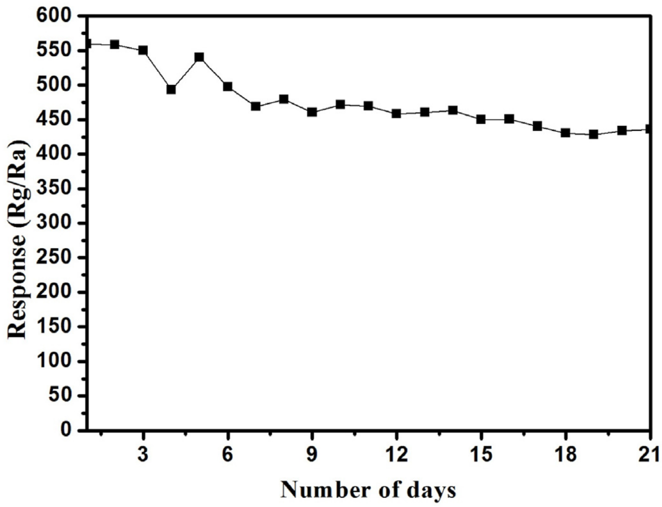

Fig. 9. Variation in the response of 3 at% Ag–ZnO based sensor to 100 ppm C_2H_2 at 175 °C over time.

highest. The result could be interpreted by the catalytic effect of Ag and the selective adsorption of C_2H_2. When Ag–ZnO nanorods were exposed to air, the surface of ZnO would absorb more oxygen molecules and more electrons in the conduction band would be trapped due to the spillover effect of Ag. At 175 °C, the catalytic effect of Ag played a significant role in catalyzing the decomposition of acetylene which might be an exothermic and spontaneous process [37]. For the gases with higher bond energy than C_2H_2 such as C_2H_5OH, CH_3COCH_3, etc., the temperature was not enough to provide the activation energy and the catalytic effect of Ag was not significant. For H_2, NO_2, and other gases with lower bond energy, the low response may be attributed to the weak strength of the interaction between the sensing materials and gases [37,38]. When sensor was operating at 250 °C, the adsorption strength of Ag–ZnO nanorods materials to C_2H_2 decreased, that made the response decrease. However, for C_2H_5OH, CH_3COCH_3, and other gases, there was enough energy to catalyze decomposition, so as to improve the response. Therefore, the selectivity at 175 °C was better than that at 250 °C.

The long-term stability result was obtained by continuous test of the response to C_2H_2 for 21 days. The response of 3 at% Ag–ZnO based sensor over time shown in Fig. 9. At the beginning, the response value decayed with time, and finally stabilized at 450, and a response attenuation of less than 25% was acceptable.

In practical applications, response, response and recovery speed, detection limit, and selectivity should be considered comprehensively. Compared with semiconductor oxides based gas sensors in previous papers, the C_2H_2 sensing performance of Ag–ZnO nanorods has advantages in sensitivity, operation temperatures, and response speed (Table 1).

3.3. Sensing mechanism

The semiconductor oxide based sensor could be divided into two kinds including surface conductivity type and bulk conductivity type from the conductive mechanism, and the gas sensing mechanism in this paper can be explained by surface conductivity type which means that the interaction between test gases and sensors only occurs on the surface of the sensing materials. The O_2 in the air would be absorbed on the surface of ZnO materials upon ZnO exposing to air, and electrons in ZnO conduction bands would be captured to form O_2^-, O^- and O^{2-} [39]. The result is a depletion layer and increase in the resistance [40].

The formation of reactive chemisorption oxygen is controlled by temperature [41]. O_2^- is generally chemisorbed at below 100 °C, O^- is generally chemisorbed at different temperature from 100 to 300 °C, and O^{2-} is generally chemisorbed at over 300 °C. In our study, all sensors worked at temperatures below 300 °C, so O^- species were mainly involved in sensing behavior. When C_2H_2 was detected, the reaction would occur on the surface of sensors as Eq. (1):

$$C_2H_2 + 5O^- \rightarrow 2CO_2 + H_2O + 5e^- \quad (1)$$

The trapped electrons would release back to ZnO materials, reducing the resistance.

Compared with ZnO based sensor, all of Ag–ZnO nanorods based sensors presented higher sensitivity to C_2H_2 which is ascribed to the electronic sensitization and chemical effect of Ag. Fig. 10 shows the scheme of sensing mechanism. Ag has high catalytic activity for the formation of active oxygen molecules (O^-) [42] adsorbed on the surface of ZnO, the O^- species play a critical role in the gas sensing of sensors by regulating the reaction with tested gases [43]. Pure ZnO and 3 at% Ag–ZnO powder were investigated by XPS to confirm the ratio of the chemisorbed oxygen in the samples. The O1s spectra shows that the chemisorbed oxygen species content (34.5%) of 3 at% Ag–ZnO is higher than that of pure ZnO (28.8%), which is mainly due to the spillover effect of Ag [44]. Ag increases the number and reaction activity of chemically adsorbed oxygen, thus increasing the response of the sensor [45]. Moreover, the Schottky junction can be formed at the interface between ZnO and Ag due to the difference in Fermi level. When Ag–ZnO material is exposed to the atmosphere, compared with pure ZnO, due to the existence of Schottky junction and the increase of O^-, the electrons in the ZnO conduction band are further reduced, thus increasing the width of depletion layer and increasing the resistance. When the Ag–ZnO material is exposed to C_2H_2, the Schottky junction produces more overflow electrons and donates it to the ZnO matrix, resulting in efficient modulation of the depletion layer [45]. In addition, due to the increase of O^-, the reaction indicated in Eq. (1) is enhanced, resulting in more trapped electrons would release back to ZnO materials and a greater reduction in resistance. Thus, the response was remarkably improved.

4. Conclusions

In summary, ZnO and Ag modified ZnO nanorods with different amounts (1 at%, 2 at%, and 3 at%) were prepared by using

Table 1
Performances of Semiconductor oxides based sensors in detecting C_2H_2.

Sensing materials	Operating temperature (°C)	Acetylene concentration (ppm)	Response (R_a/R_g)	Response/Recovery speed	Refs.
Ni–ZnO	350	200	34.7	15s/19s	[5]
Ni/ZnO	250	2000	17	5s/10s	[6]
Ag/ZnO/rGO	90	50	13%	235s/16s	[7]
Sm_2O_3/SnO_2	260	100	50.5	8s/9s	[8]
Ag/ZnO	200	100	14	57s/36s	[37]
ZnO	275	100	16	15s/87s	This work
Ag–ZnO	175	100	539	6s/1.5 h	This work
Ag–ZnO	250	100	255	6s/200s	This work

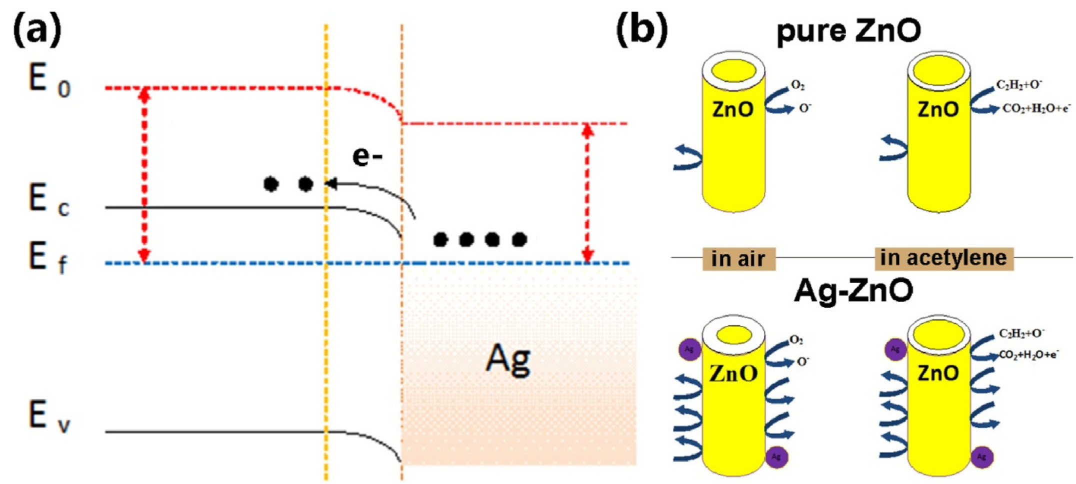

Fig. 10. Energy band diagram of Ag–ZnO nanorods (a); the scheme of sensing mechanism (b).

solvothermal process. Sensing properties including response, repeatability, selectivity and response speed to C_2H_2 of Ag–ZnO based sensors were superior to ZnO and other semiconductor oxides based gas sensors in literatures, and two solutions were proposed to accelerate the recovery process. The underlying sensing mechanism and reason of improving gas sensing performance by Ag modification was proposed.

Declaration of competing interest

The authors declare that they have no known competing financial interestsor personal relationships that could have appeared to influence the work reported in this paper.

Acknowledgement

This work is supported by National Natural Science Foundation of China (Nos. 61871198, 61831011, and 61520106003).

References

[1] A.B. Antonsson, B. Christensson, J. Berge, B. Sjögren, Fatal carbon monoxide intoxication after acetylene gas welding of pipes, Ann. Occup. Hyg. 57 (2013) 662–666.
[2] J. Steinmetz, H.J. Lee, S. Kwon, D.S. Lee, C. Goze-Bac, E. Abou-Hamad, H. Kim, Y.W. Park, Routes to the synthesis of carbon nanotube-poly acetylene composites by Ziegler-Natta polymerization of acetylene inside carbon nanotubes, Curr. Appl. Phys. 7 (2007) 39–41.
[3] R. Saroha, A.K. Panwar, Effect of in situ pyrolysis of acetylene (C_2H_2) gas as a carbon source on the electrochemical performance of $LiFePO_4$ for rechargeable lithium-ion batteries, J. Phys. D Appl. Phys. 50 (2017) 255501.
[4] D.C. Bastos, A.E.F. Dos Santos, R.A. Simao, Acetylene coating on cornstarch plastics produced by cold plasma technology, Starch Staerke 66 (2014) 267–273.
[5] W.G. Chen, T.Y. Gao, H.L. Gan, L.N. Xu, L.F. Jin, Improved C_2H_2 sensing properties of Ni doped ZnO nanorods, Mater. Technol. 30 (2015) 356–361.
[6] X.C. Wang, M.G. Zhao, F. Liu, J.F. Jia, X.J. Li, L.L. Cao, C_2H_2 gas sensor based on Ni doped ZnO electrospun nanofibers, Ceram. Int. 39 (2013) 2883–2887.
[7] C.X. Jiang, D.Z. Zhang, N.L. Yin, Y. Yao, T. Shaymurat, X.Y. Zhou, Acetylene gas sensing properties of layer-by-layer self-assembled Ag-decorated Tin dioxide/graphene nanocomposite film, Nanomaterials 7 (2017) 278.
[8] Q. Zhou, C. Tang, S.P. Zhu, W.G. Chen, J. Li, Synthesis, characterization and sensing properties of Sm_2O_3 doped SnO_2 nanorods to C_2H_2 gas extracted from power transformer oil, Mater. Technol. 31 (2016) 364–370.
[9] Z. Wu, Y. Gong, Q. Yu, Photoacoustic spectroscopy detection and extraction of discharge feature gases in transformer oil based on 1.5 mu tunable fiber laser, Infrared Phys. Technol. 58 (2013) 86–90.
[10] N. Maksymovych, O. Ripko, O. Maksymovych, O. Kaskevych, N. Nikitina, V. Ruchko, O. Kuzko, V. Yatsimirsky, Adsorption semiconductor detector for malfunction diagnosis of high voltage transformers, Sensor. Actuator. B Chem. 93 (2003) 321–326.
[11] C.L. Wang, A. Liu, X.L. Yang, J. Wang, R. You, Z.J. Yang, J.M. He, L.J. Zhao, F.M. Liu, X. Yan, X.S. Liang, Y. Gao, F.M. Liu, P. Sun, G.Y. Lu, YSZ-based mixed-potential type highly sensitive acetylene sensor based on porous SnO_2/Zn_2SnO_4 as sensing electrode, Sensor. Actuator. B Chem. 293 (2019) 116–172.
[12] M. Bagheri, N.F. Hamedani, A.R. Mahjoub, A.A. Khodadadi, Y. Mortazavi, Highly sensitive and selective ethanol sensor based on Sm_2O_3-loaded flower-like ZnO nanostructure, Sensor. Actuator. B Chem. 191 (2014) 283–290.
[13] G.Y. Lu, J. Xu, J.B. Sun, Y.S. Yu, Y.Q. Zhang, F.M. Liu, UV-enhanced room temperature NO_2 sensor using ZnO nanorods modified with SnO_2 nanoparticles, Sensor. Actuator. B Chem. 162 (2012) 82–88.
[14] Q. Zhou, L.N. Xu, A. Umar, W.G. Chen, R. Kumar, Pt nanoparticles decorated SnO_2 nanoneedles for efficient CO gas sensing applications, Sensor. Actuator. B Chem. 256 (2018) 656–664.
[15] Q. Zhou, W.G. Chen, J. Li, C. Tang, H. Zhang, Nanosheet-assembled flower-like SnO_2 hierarchical structures with enhanced gas-sensing performance, Mater. Lett. 161 (2015) 499–502.
[16] Y.Q. Li, A novel snowflake-like SnO_2 hierarchical architecture with superior gas sensing properties, Physica 96 (2018) 54–56.
[17] Q. Zhou, C. Tang, S.P. Zhu, W.G. Chen, NiO doped SnO_2 p-n heterojunction microspheres: preparation, characterization and CO sensing properties, Mater. Technol. 30 (2015) 349–355.
[18] Z.P. Tshabalala, D.E. Motaung, H.C. Swart, Structural transformation and enhanced gas sensing characteristics of TiO_2 nanostructures induced by annealing, Physica B 535 (2018) 227–231.
[19] F.J. Pan, H. Lin, H.Z. Zhai, Z. Miao, Y. Zhang, K.L. Xu, B. Guan, H. Huang, H. Zhang, Pd-doped TiO_2 film sensors prepared by premixed stagnation flames for CO and NH_3 gas sensing, Sensor. Actuator. B Chem. 261 (2018) 451–459.
[20] H.L. Tian, H.Q. Fan, H. Guo, N. Song, Solution – based synthesis of ZnO/carbon nanostructures by chemical coupling for high performance gas sensors, Sensor. Actuator. B Chem. 195 (2014) 132–139.
[21] J.P. Ma, J. Ren, Y.M. Jia, Z. Wu, L. Chen, Neale O. Haugen, H.T. Huang, Y.S. Liu, High efficiency bi-harvesting light/vibration energy using piezoelectric zinc oxide nanorods for dye decomposition, Nanomater. Energy 62 (2019) 376–383.
[22] X.L. Xu, Y.M. Jia, L.B. Xiao, Zheng Wu, Strong vibration-catalysis of ZnO nanorods for dye wastewater decolorization via piezo-electro-chemical coupling, Chemosphere 193 (2018) 1143–1148.
[23] X. Zhang, J. Qin, Y. Xue, P. Yu, B. Zhang, L. Wang, R. Liu, Effect of aspect ratio and surface defects on the photocatalytic activity of ZnO nanorods, Sci. Rep. 4 (2014) 4596.
[24] H.L. You, Z. Wu, Y.M. Jia, X.L. Xu, Y.T. Xia, Z.C. Han, Y. Wang, High-efficiency and mechano-/photo- bi-catalysis of piezoelectric-ZnO@ photoelectric-TiO_2 core-shell nanofibers for dye decomposition, Chemosphere 183 (2017) 528–535.
[25] W.Q. Qian, Z. Wu, Y.M. Jia, Y.T. Hong, X.L. Xu, H.L. You, Y.Q. Zheng, Y.T. Xia, Thermo-electrochemical coupling for room temperature thermocatalysis in pyroelectric ZnO nanorods, Electrochem. Commun. 81 (2017) 124–127.
[26] N.N.K. Truong, T.N. Trung, N. Tu, N.V. Nghia, D.M. Thuy, Preparation and characterization of Ag doped ZnO nanostructure, Int. J. Nanotechnol. 10 (2013) 260–268.
[27] M. Arab Chamjangali, G. Bagherian, A. Javid, S. Boroumand, N. Farzaneh, Spectrochim. Synthesis of Ag–ZnO with multiple rods (multipods) morphology and its application in the simultaneous photo-catalytic degradation of methyl orange and methylene blue, Acta Part A: Mol. Biomol. Spectrosc. 150 (2015) 230–237.
[28] Y. Zheng, L. Zheng, Y. Zhan, X. Lin, Q. Zheng, K. Wei, Ag/ZnO heterostructure Nanocrystals: synthesis, characterization, and photocatalysis, Inorg. Chem. 46 (2007) 6980–6986.
[29] F. Sun, X. Qiao, F. Tan, W. Wang, X. Qiu, One-step microwave synthesis of Ag/ZnO nanocomposites with enhanced photocatalytic performance, J. Mater. Sci. 47 (2012) 7262–7268.
[30] K. Saoud, R. Alsoubaihi, N. Bensalah, T. Bora, M. Bertino, J. Dutta, Synthesis of supported silver nano-spheres on zinc oxide nanorods for visible light photocatalytic applications, Mater. Res. Bull. 63 (2015) 134–140.
[31] Z.Y. Zhang, C.L. Shao, X.H. Li, C.H. Wang, M.Y. Zhang, Y.C. Liu, Electrospun nanofibers of p-Type NiO/n-type ZnO heterojunctions with enhanced photocatalytic

activity, ACS Appl. Mater. Interfaces 10 (2010) 2915–2923.
[32] L.W. Wang, Y.F. Kang, Y. Wang, B.L. Zhu, S.M. Zhang, W.P. Huang, S.R. Wang, CuO nanoparticle decorated ZnO nanorod sensor for low-temperature H_2S detection, Mater. Sci. Eng. C 32 (2012) 2079–2085.
[33] X. Liu, B.S. Du, Y. Sun, M. Yu, Y.Q. Yin, W. Tang, C. Chen, L. Sun, B. Yang, W.W. Cao, Michael N.R. Ashfold, Sensitive room temperature photoluminescence-based sensing of H_2S with novel CuO-ZnO nanorods, ACS Appl. Mater. Interfaces 8 (2016) 16379–16385.
[34] D. Li, Y.Q. Zhang, D.Y. Liu, S.T. Yao, F.M. Liu, B. Wang, P. Sun, Y. Gao, X.H. Chuai, G.Y. Lu, Hierarchical core/shell ZnO/NiO nanoheterojunctions synthesized by ultrasonic spray pyrolysis and their gas-sensing performance, CrystEngComm 18 (2016) 8101–8107.
[35] C. Wang, X.B. Cui, J.Y. Liu, X. Zhou, X.Y. Cheng, P. Sun, X.L. Hu, X.W. Li, J. Zheng, G.Y. Lu, Design of superior ethanol gas sensor based on Al-doped NiO nanorod-Flowers, ACS Sens. 1 (2016) 131–136.
[36] W. Kim, M. Choi, K. Yong, Generation of oxygen vacancies in ZnO nanorods/films and their effects on gas sensing properties, Sens. Actuators, B 209 (2015) 989–996.
[37] A.S.M. Iftekhar Uddin, Usman Yaqoob, Duy-Thach Phan, Gwiy-Sang Chung*, A novel flexible acetylene gas sensor based on PI/PTFE-supported Ag-loaded vertical ZnO nanorods array, Sensor. Actuator. B Chem. 222 (2016) 536–543.
[38] Z.S. Hosseinia, A. Irajizad, A. Mortezaali, Room temperature H2S gas sensor based on rather aligned ZnO nanorods with flower-like structures, Sensor. Actuator. B Chem. 207 (2015) 865–871.
[39] N. Yamazoe, K. Shimanoe, Theory of power laws for semiconductor gas sensors, Sensor. Actuator. B Chem. 128 (2008) 566–573.
[40] L.P. Gao, F.M. Ren, Z.X. Cheng, Y. Zhang, Q. Xiang, J.Q. Xu, Porous corundum-type In_2O_3 nanoflowers: controllable synthesis, enhanced ethanol-sensing properties and response mechanism, CrystEngComm 17 (2015) 3268–3276.
[41] J. Zhang, S.R. Wang, Y. Wang, M.J. Xu, H.J. Xia, S.M. Zhang, W.P. Huang, X.Z. Guo, S.H. Wu, Facile synthesis of highly ethanol-sensitive SnO_2 nanoparticles, Sensor. Actuator. B Chem. 139 (2009) 369–374.
[42] J. Guo, J. Zhang, M. Zhu, D. Ju, H. Xu, B. Cao, High-performance gas sensor based on ZnO nanowires functionalized by Au nanoparticles, Sensor. Actuator. B Chem. 199 (2014) 339–345.
[43] L. Gao, F. Ren, Z. Cheng, Y. Zhang, Q. Xiang, J. Xu, Porous corundumtype In_2O_3 nanoflowers: controllable synthesis, enhanced ethanol-sensing properties and response mechanism, CrystEngComm 17 (2015) 3268–3276.
[44] M. Hubner, D. Koziej, J.D. Grunwaldt, U. Weimar, N. Barsan, An Au clusters related spill-over sensitization mechanism in SnO_2-based gas sensors identified by operando HERFD-XAS, work function changes, DC resistance and catalytic conversion studies, Phys. Chem. Chem. Phys. 14 (2012) 13249–13254.
[45] S.Q. Zhou, M.P. Chen, Q.J. Lu, Y.M. Zhang, J. Zhang, B. Li, H.T. Wei, J.C. Hu, H.P. Wang, Q.G. Liu, Ag nanoparticles sensitized In_2O_3 nanograin for the ultrasensitive HCHO detection at room temperature, Nanoscale Res. Lett. 14 (2019) 365.